

Cationic helicenes as selective G4 DNA binders and optical probes for cellular imaging

Peter A. Summers,^{1#} Ajesh P. Thomas,^{1#} Timothy Kench, Jean-Baptiste Vannier,^{2,3} Marina K. Kuimova*,¹ Ramon Vilar*¹

Supplementary Information

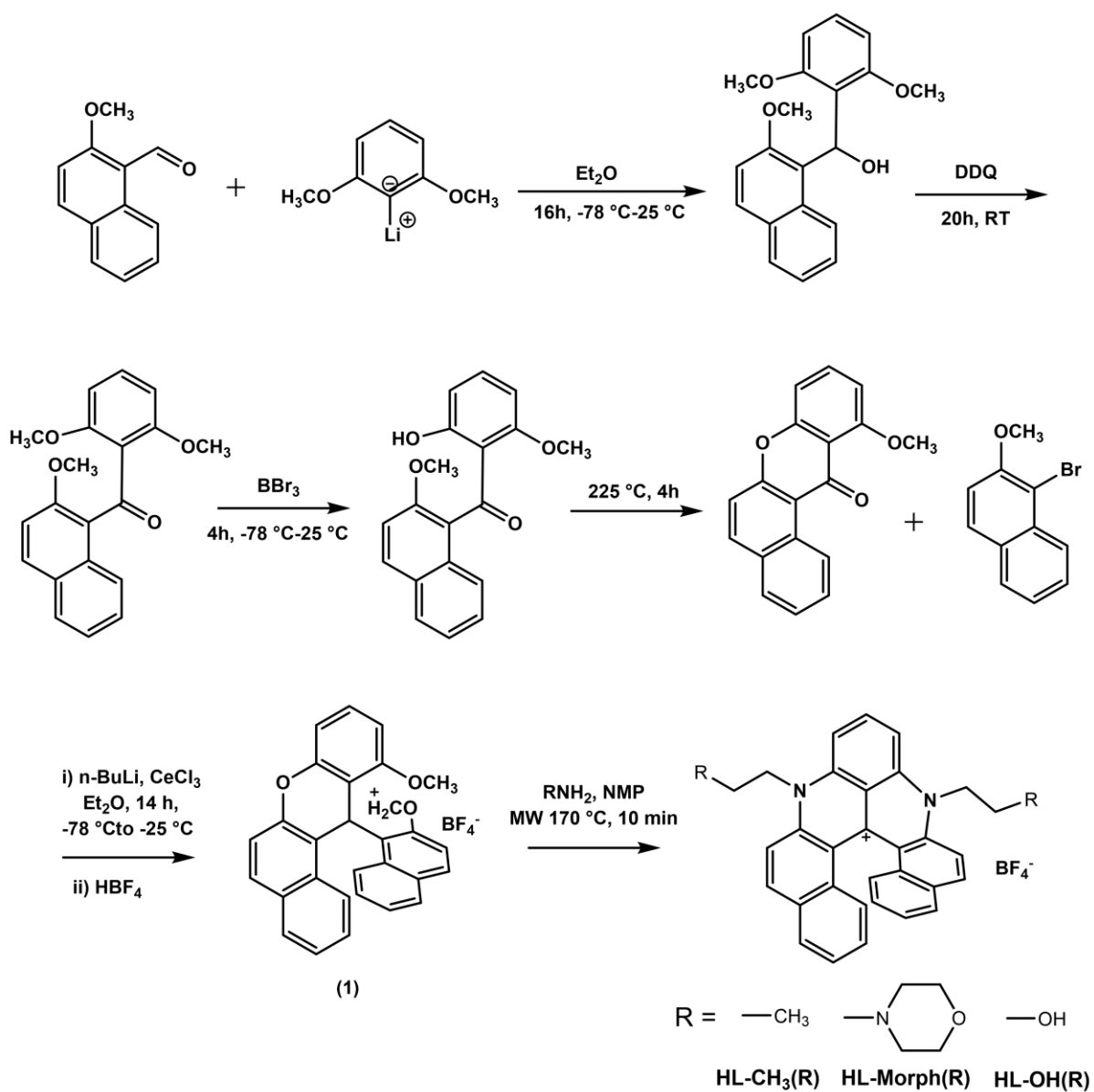


Figure S1. Synthetic pathway to HL-CH₃(R), HL-Morph(R), and HL-OH(R).

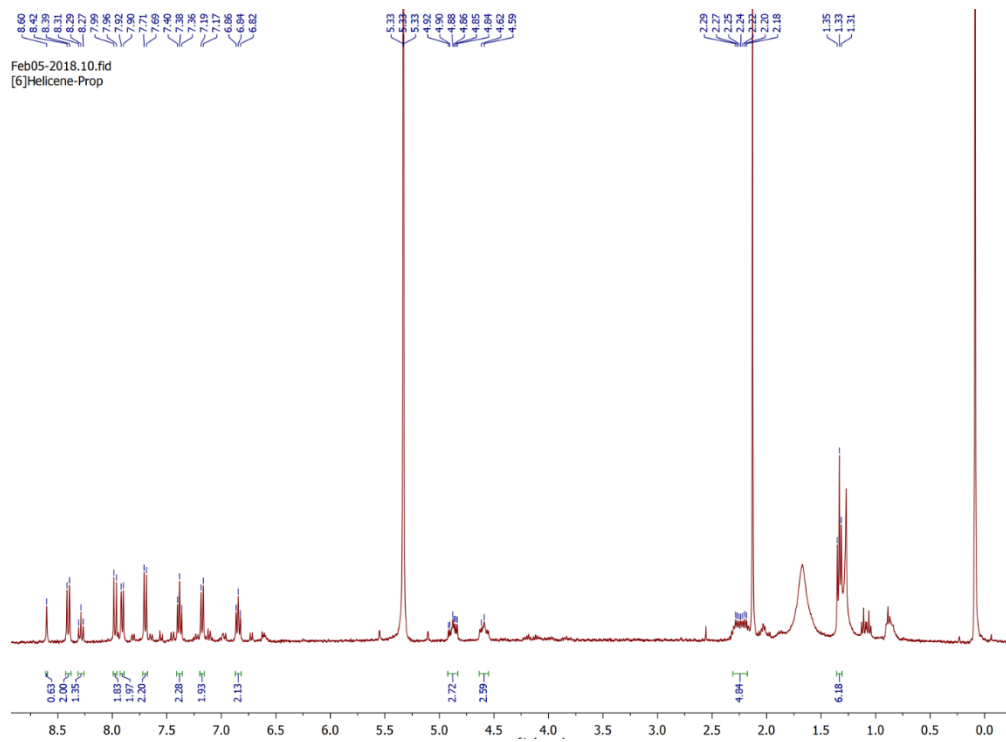


Figure S2. ^1H NMR spectrum of HL-CH₃(R) in CD₃OD.

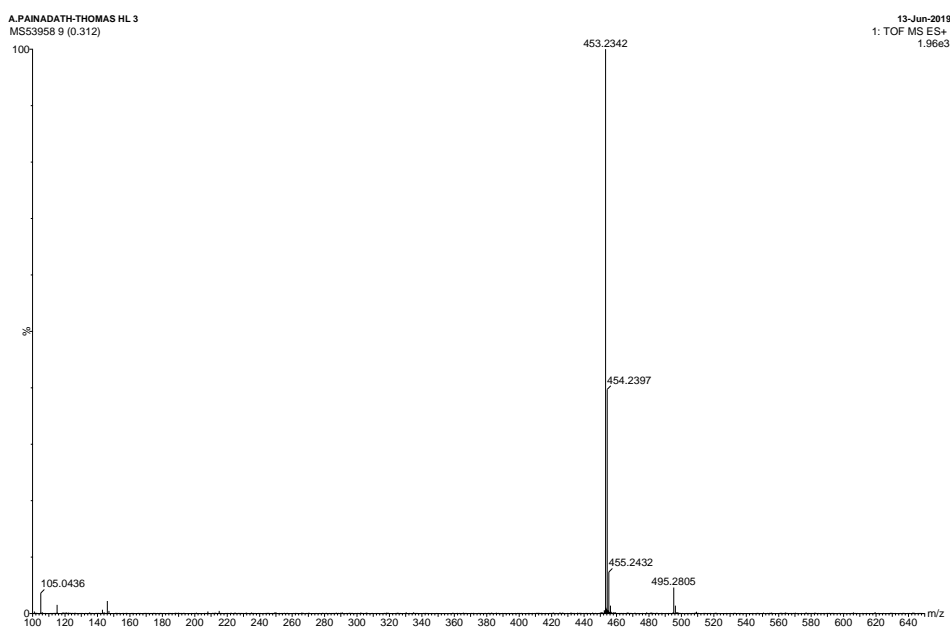


Figure S3. ESI-MS spectrum of HL-CH₃(R).

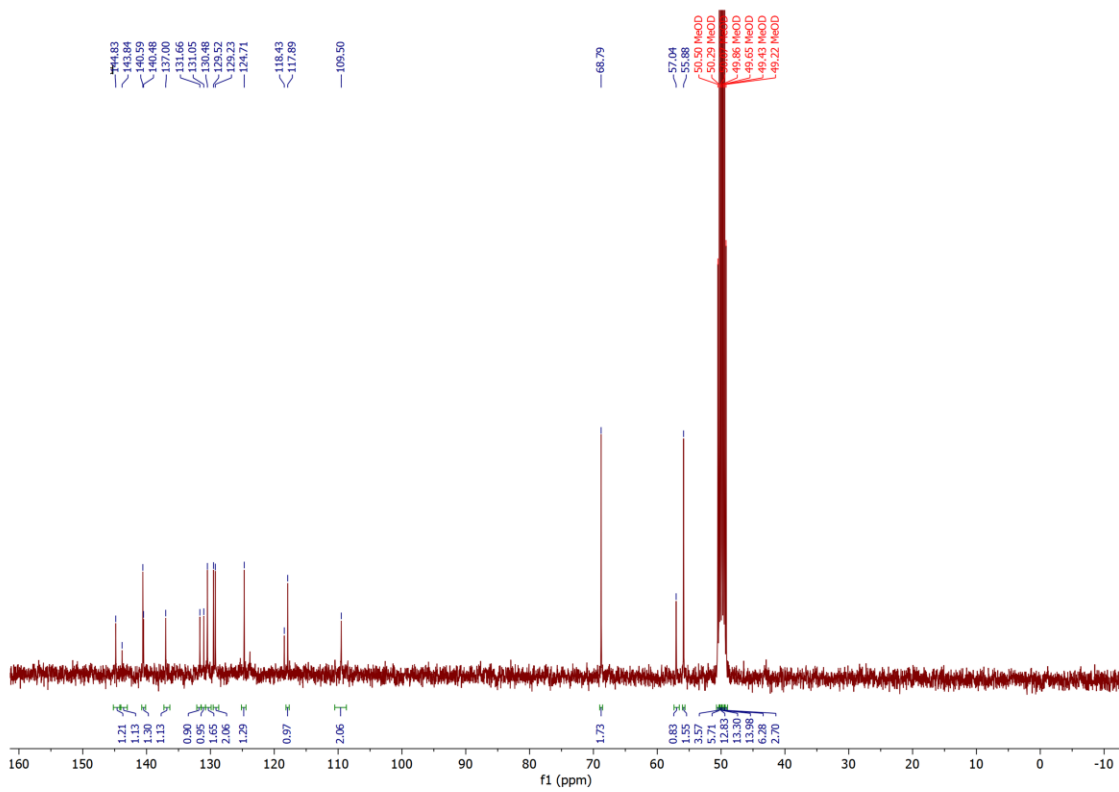
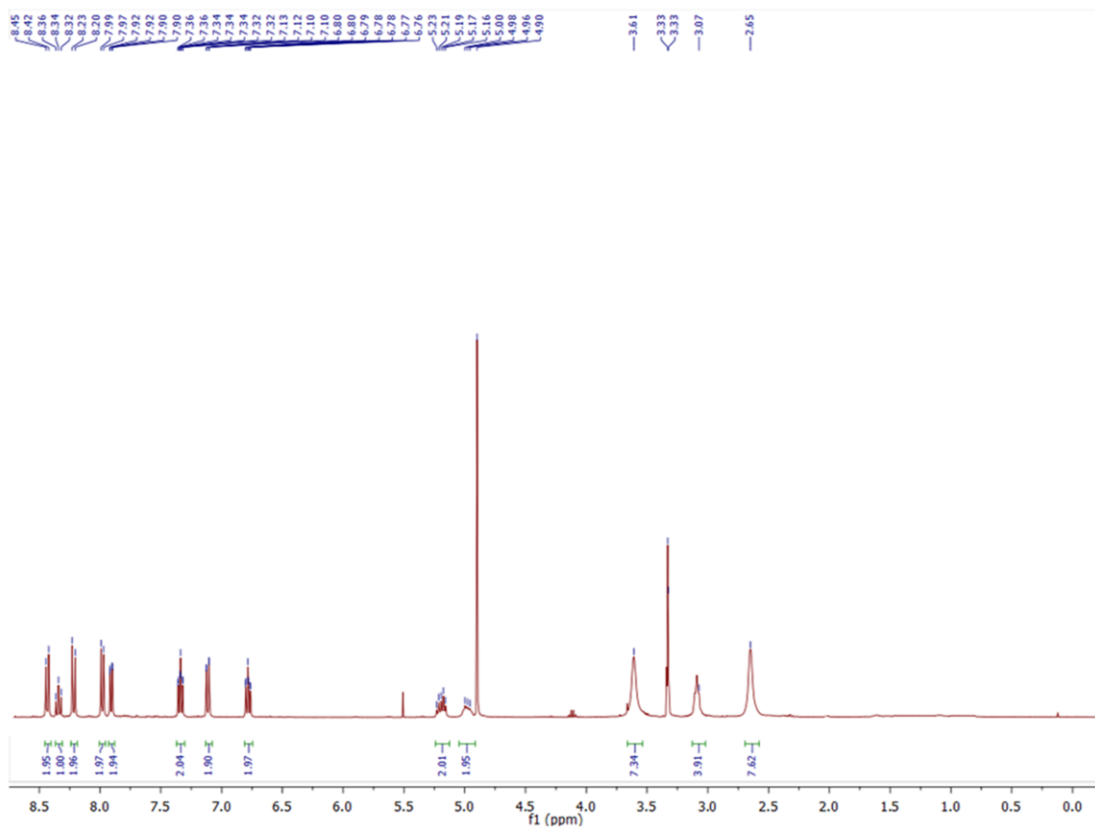


Figure S4. ¹H NMR (top) and ¹³C NMR (bottom) spectra of HL-Morph(R) in CD₃OD.

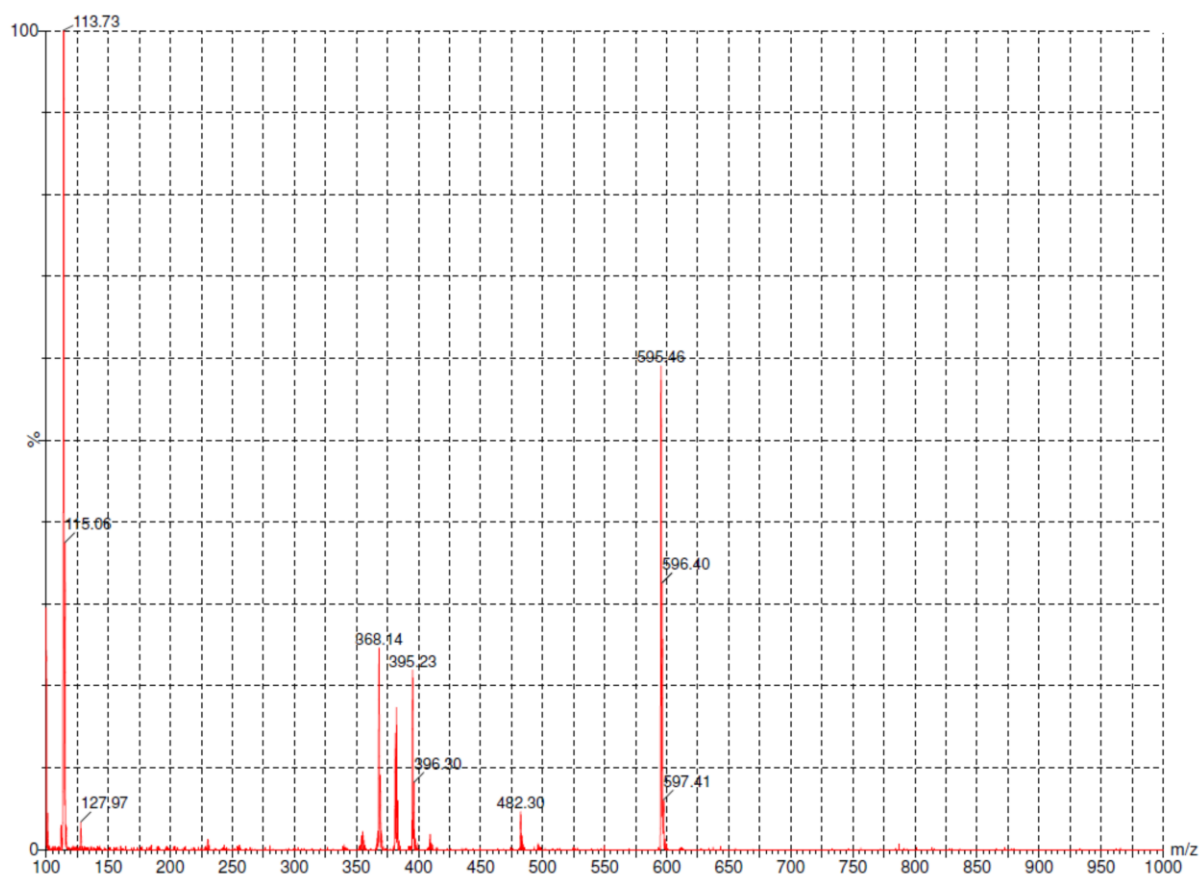


Figure S5. ESI-MS spectrum of HL-Morph(R).

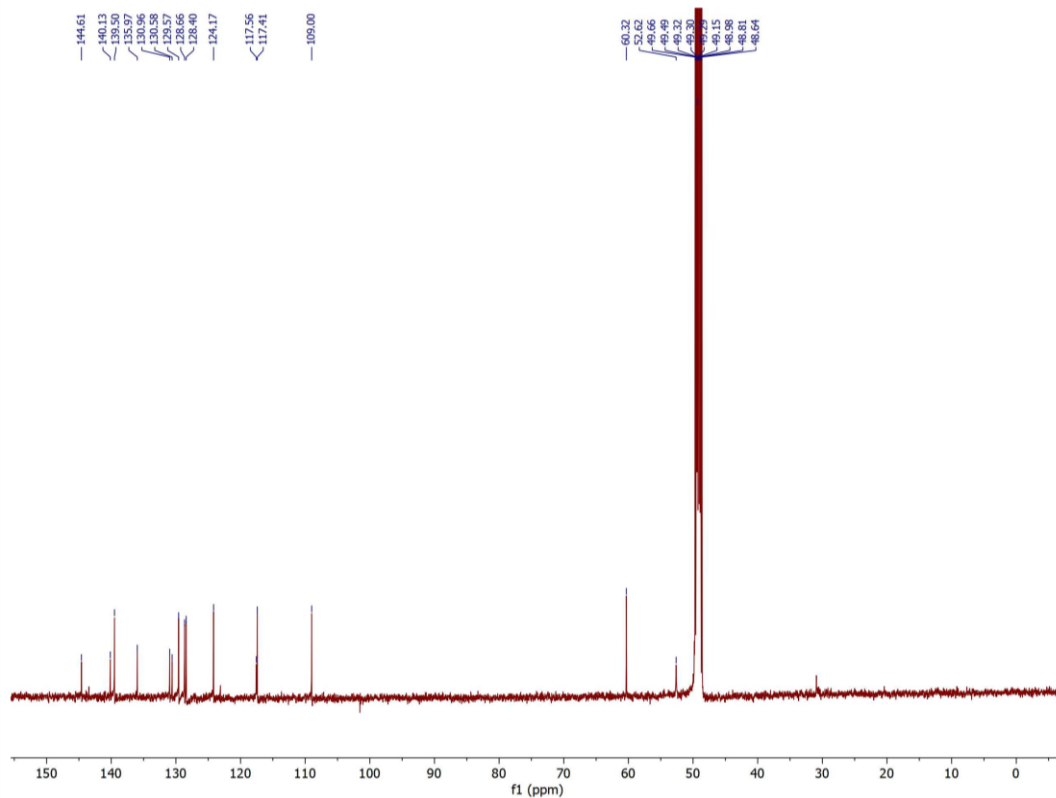
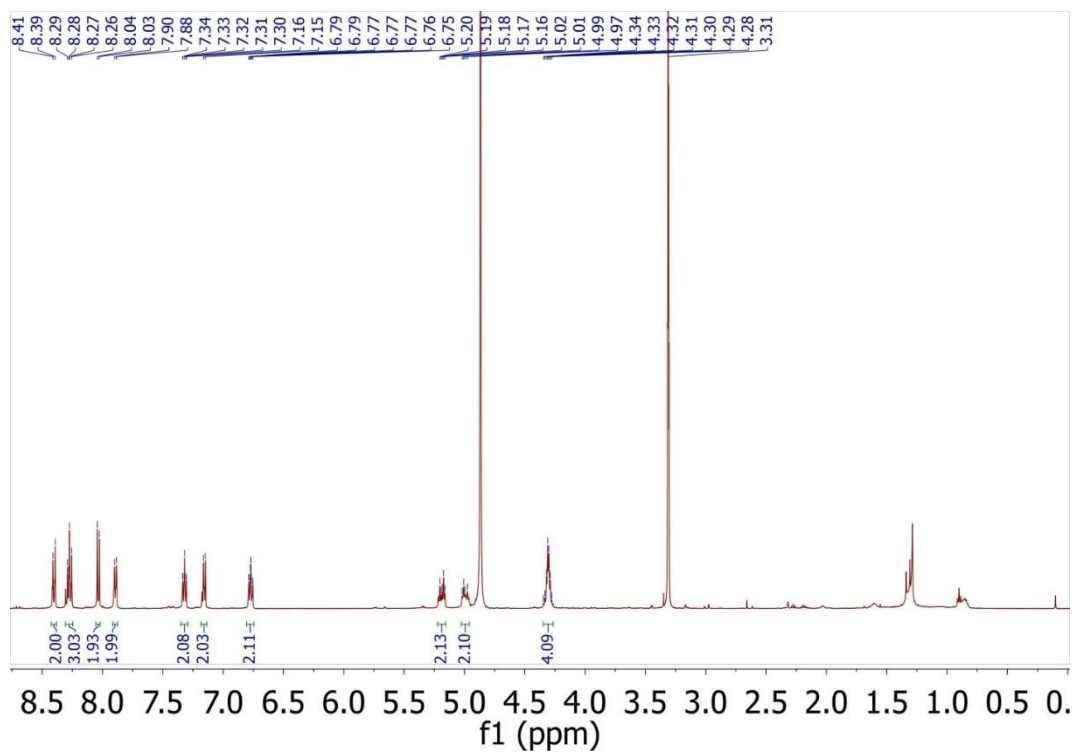


Figure S6. ^1H NMR (top) and ^{13}C NMR (bottom) spectra of **HL-OH(R)** in CD_3OD .

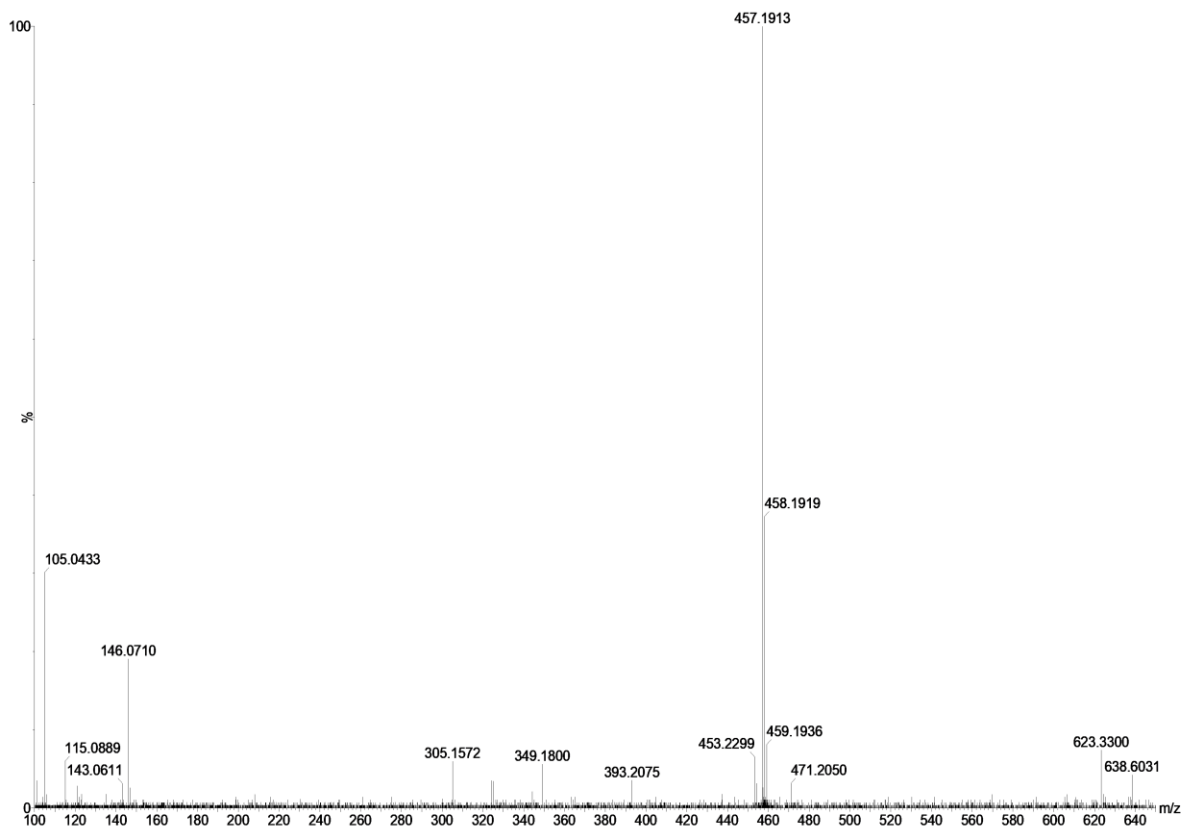


Figure S7. ESI-MS spectrum of HL-OH(R).

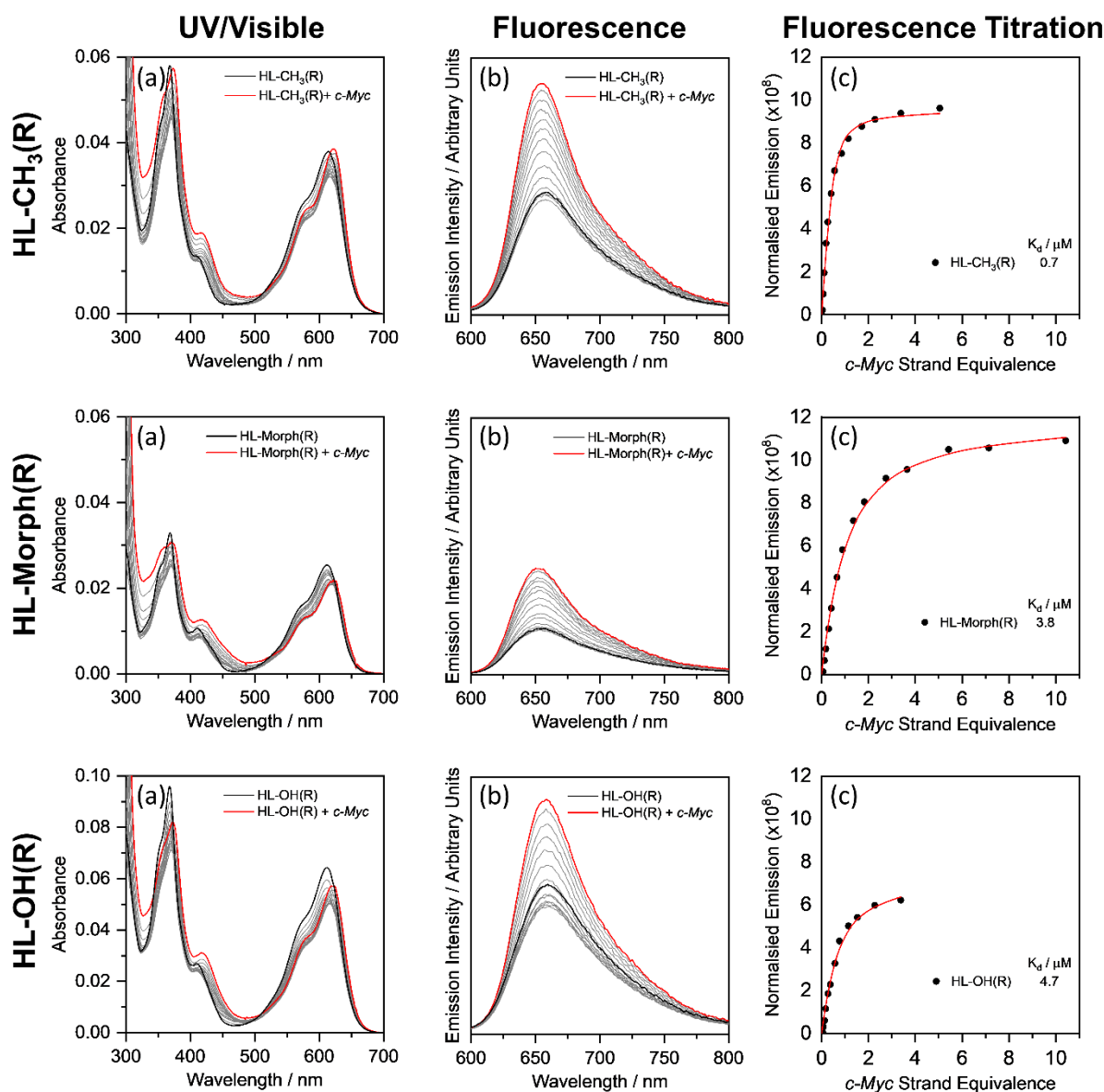


Figure S8. Titration spectra and simple binding affinities of **HL-CH₃(R)** (4 μM), **HL-Morph(R)** (2.5 μM), and **HL-OH(R)** (6 μM) to *c-Myc* G4 DNA. (a) Absorption spectra and (b) Fluorescence spectra ($\lambda_{\text{ex}} = 580 \text{ nm}$, $\lambda_{\text{em}} = 600\text{-}700 \text{ nm}$) during addition of *c-Myc*. (c) Difference in Integrated emission during titration. Integrated intensities are normalised against absorption at the excitation wavelength. The solid red line is a best fit of a simple binding model. All experiments in 10 mM lithium cacodylate buffer (pH 7.3) with 100 mM KCl.

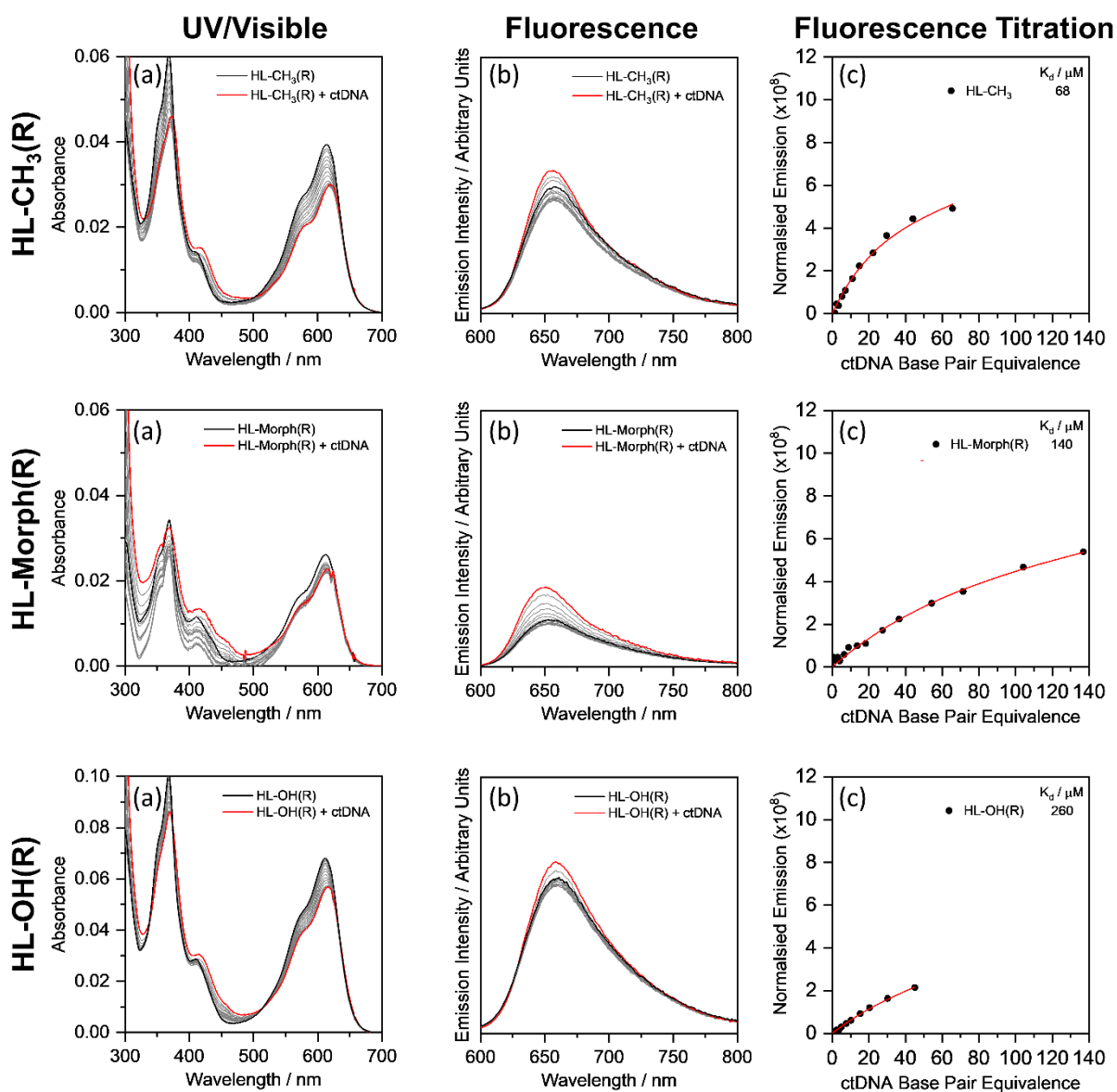
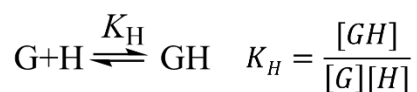


Figure S9. Titration spectra and simple binding affinities of **HL-CH₃(R)** (4 μM), **HL-Morph(R)** (2.5 μM), and **HL-OH(R)** (6 μM) to ctDNA DNA. (a) Absorption spectra and (b) Fluorescence spectra ($\lambda_{\text{ex}} = 580 \text{ nm}$, $\lambda_{\text{em}} = 600\text{-}700 \text{ nm}$) during addition of ctDNA DNA. (c) Difference in Integrated emission during titration. Integrated intensities are normalised against absorption at the excitation wavelength. The solid red line is a best fit of a simple binding model. All experiments in 10 mM lithium cacodylate buffer (pH 7.3) with 100 mM KCl.

Simple

Equilibria



$$[G]_0 = [G] + [GH]$$

$$[H]_0 = [H] + [GH]$$

Guest Concentration

$$a[G]^2 + b[G] + c = 0$$

$$a = 1$$

$$b = -[G]_0 + [H]_0 + K_H^{-1}$$

$$c = -[G]_0 \times K_H^{-1}$$

Fluorescence Change

$$\Delta F = k_{\Delta GH} [GH]$$

Competitive

Equilibria



$$[G]_0 = [G] + [GP] + [GM]$$

$$[P]_0 = [P] + [GP]$$

$$[M]_0 = [M] + [GM]$$

Guest Concentration

$$a[G]^3 + b[G]^2 + c[G] + d = 0$$

$$a = K_P K_M$$

$$b = K_P + K_M + K_P K_M ([M]_0 + [P]_0 - [G]_0)$$

$$c = 1 + K_P ([P]_0 - [G]_0) + K_M ([M]_0 - [G]_0)$$

$$d = -[G]_0$$

Fluorescence Change

$$\Delta F = \frac{k_{\Delta GP} K_P [G][P]_0}{1 + K_P [G]} + \frac{k_{\Delta GM} K_M [G][M]_0}{1 + K_M [G]}$$

Figure S10. Equilibrium equations used to fit titration data to either simple^{1,2} or competitive^{3,4} binding models using a modified form of the MatLab script reported previously.^{1,2} G = binding sites in the oligonucleotides (two compounds to one G-quadruplex and two compounds per five base pairs for ctDNA) as per reference 5 for **DAOTA-Morph**, H = helicene (racemic mixtures), P = **HL-OH(P)**, M = **HL-OH(M)**. $k_{\Delta GH}$ $k_{\Delta GP}$ $k_{\Delta GM}$ = difference in emission intensity between bound and free H, P and M, respectively. Fluorescence response of G assumed to be 0. No cooperativity between binding sites assumed. Titrations with **HL-OH(R)** (0% ee), **HL-OH(P)** (32% ee) and **HL-OH(M)** (96% ee) were fitted simultaneously to solve for K_P , K_M , $k_{\Delta GP}$ and $k_{\Delta GM}$.

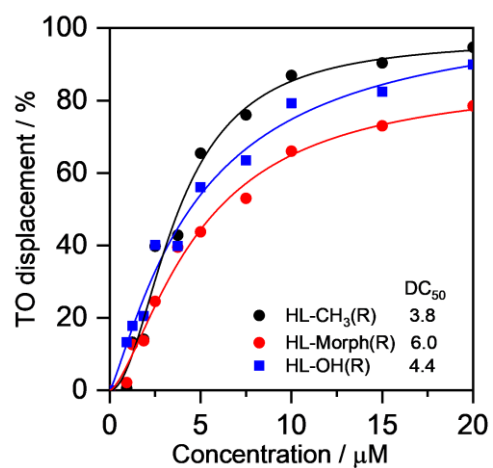


Figure S11. TO G4-FID curves for **HL- $\text{CH}_3(\text{R})$** , **HL-Morph(R)**, and **HL-OH(R)** ($\lambda_{\text{ex}} = 475 \text{ nm}$, $\lambda_{\text{em}} = 520 \text{ nm}$). Solid lines are Hill function fits of the displacement curves. All experiments in 10 mM TRIS-HCl buffer (pH 7.3) with 100 mM KCl.

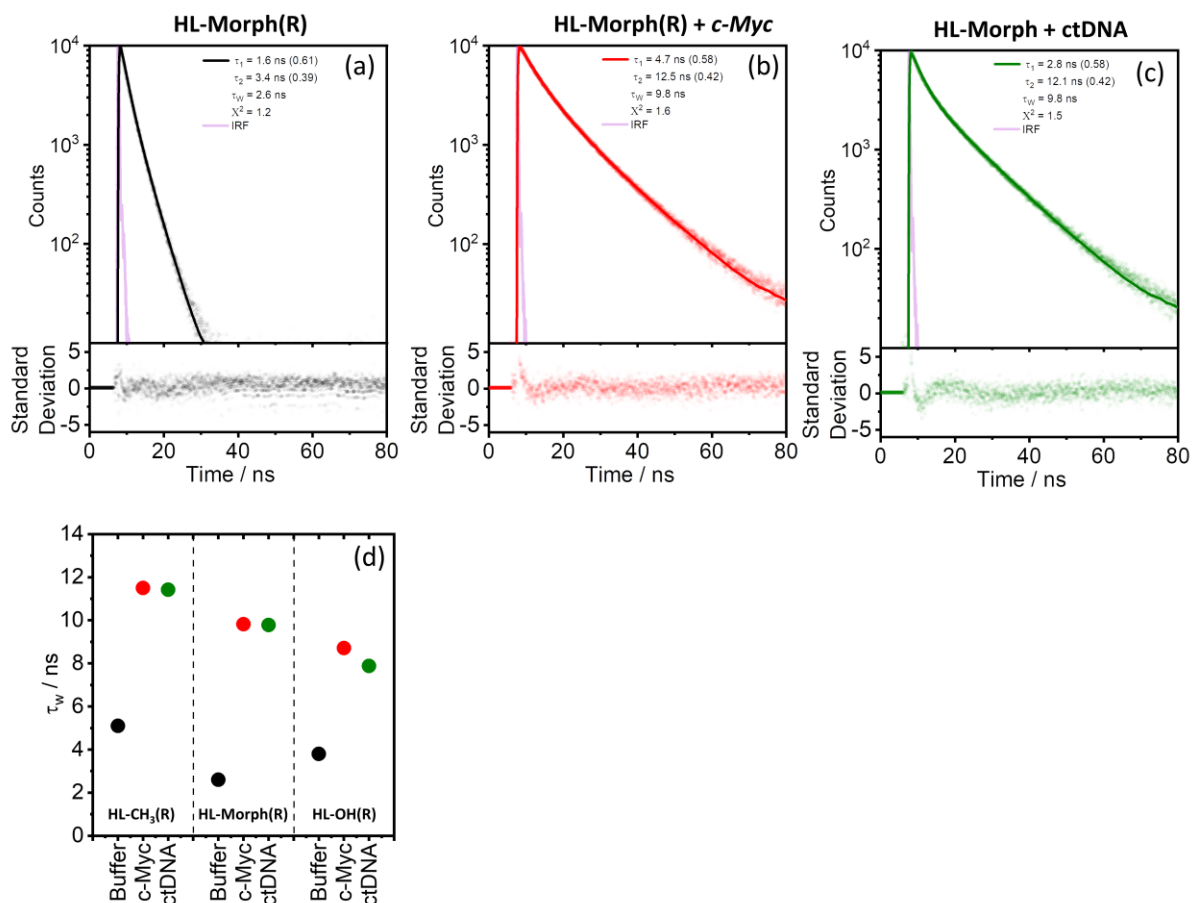


Figure S12. (a) Time resolved fluorescence decays of **HL-Morph(R)** in buffered aqueous solution and bound to different oligonucleotide topologies. G4 (*c-Myc*, 10 strand equivalence, red dots), dsDNA (ctDNA, 140 base pair equivalence, green dots) and RNA (tRNA, 140 base equivalence, blue dots). Solid lines are bi-exponential fits of the decay traces. (b) Variation in average lifetime (τ_w) of **HL-CH₃(R)**, **HL-Morph(R)**, and **HL-OH(R)** in buffered aqueous solution and when bound to *c-Myc*, and dsDNA. All experiments in 10 mM TRIS-HCl buffer (pH 7.3) with 100 mM KCl.

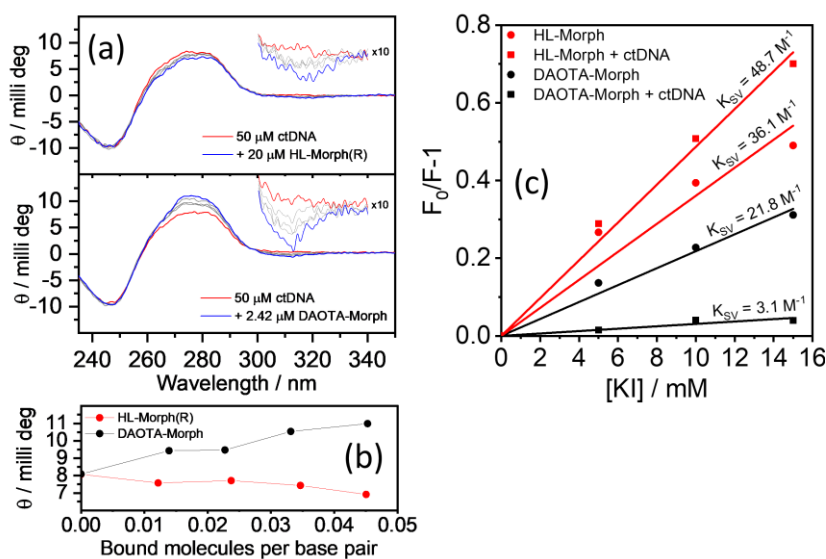


Figure S13. (a) CD spectra of ctDNA (50 μM) during addition (0 to 0.045 bound molecules per base pair) of **HL-Morph(R)** (top) and **DAOTA-Morph** (bottom). Inset: 10x expansion in the y-axis for the range 300 – 340 nm. In both titrations, the amount of dye added was calculated to keep the ratio of bound molecules per dsDNA base pair constant. (b) Change in θ at 277 nm during the titration shown in (a). (c) Quenching by KI of **HL-Morph(R)** and **DAOTA-Morph** (both at 2 μM) when 100% free dye or bound to dsDNA (818 and 11 μM , respectively). In both experiments with dsDNA, the amount of bound dye was constant at 70%. Calculations of bound dye concentrations were performed using the simple binding equation in Figure S10, and the K_d values for **HL-Morph(R)** (140 μM , Table 1) and **DAOTA-Morph** (1.3 μM , reference ⁵).

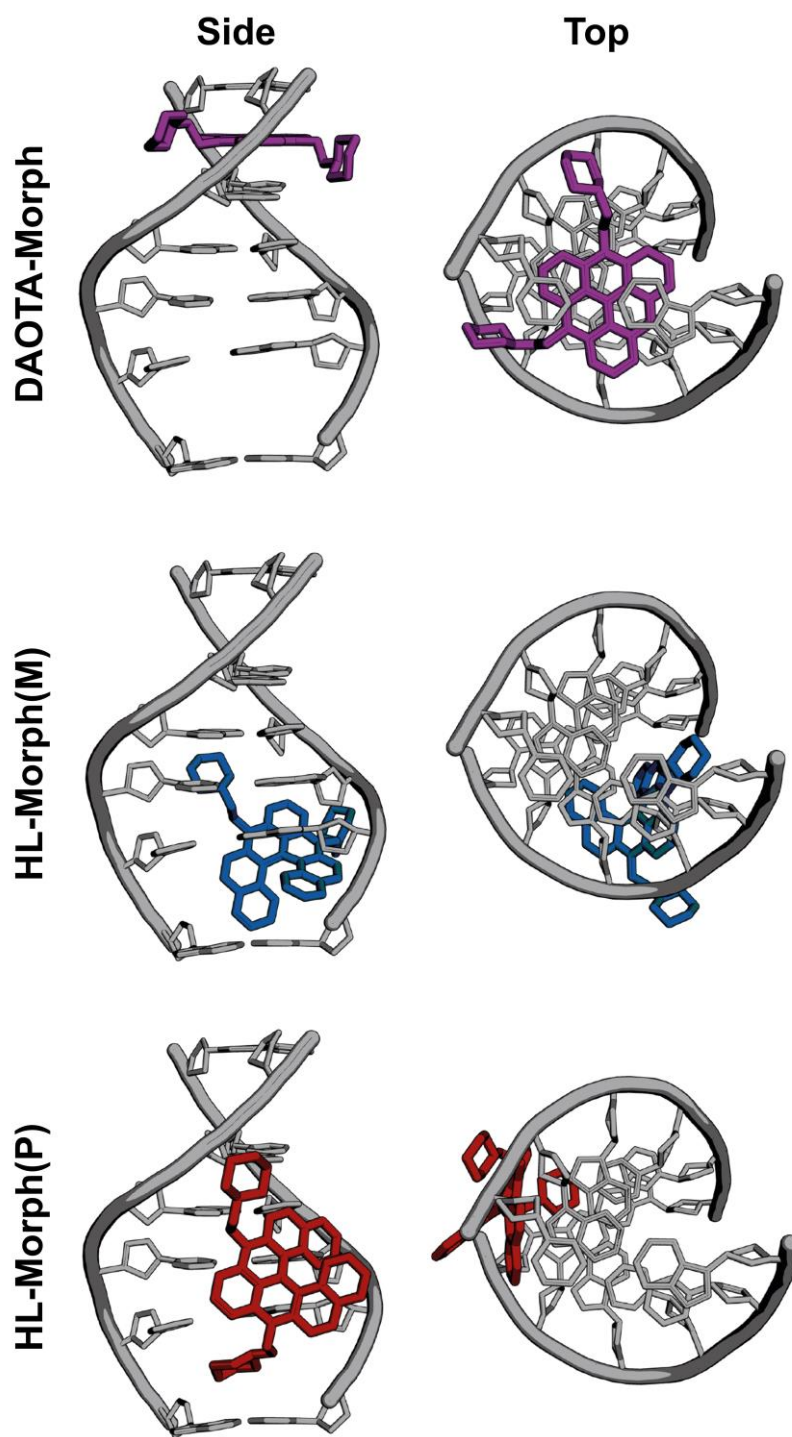


Figure S14. Lowest energy orientation following molecular docking of **HL-Morph(P)** (red), **HL-Morph(M)** (blue) and **DAOTA-Morph** (magenta) to dsDNA containing an intercalation binding site. Planar **DAOTA-Morph** can intercalate into the binding site, whereas **HL Morph(P)** (red), and **HL Morph(M)** does not fit.

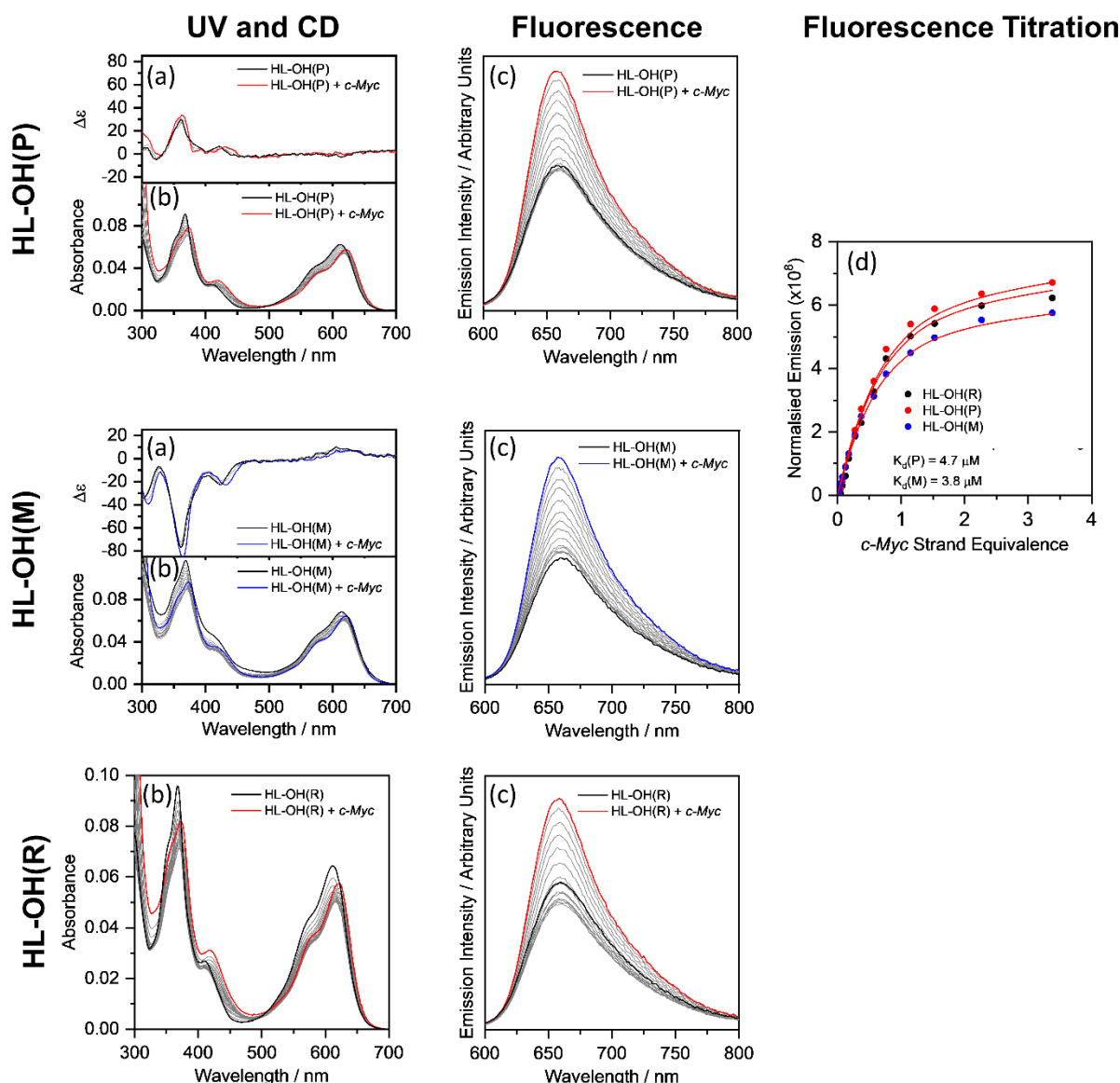


Figure S15. Titration spectra and competitive binding affinities of **HL-OH(R)** (6 μM , 0% ee), **HL-OH(P)** (6 μM , 32% ee), and **HL-OH(M)** (6 μM , 96% ee) to *c-Myc*. (a) CD spectra during addition of *c-Myc*. (b) Absorption spectra and (c) Fluorescence spectra ($\lambda_{\text{ex}} = 580 \text{ nm}$, $\lambda_{\text{em}} = 600\text{-}700 \text{ nm}$) during addition of *c-Myc*. (d) Difference in Integrated emission during titration. Integrated intensities are normalised against absorption at the excitation wavelength. The solid red lines are a simultaneous best fit of all three titrations to a competitive binding model, to solve for K_P , K_M , $k_{\Delta\text{GP}}$ and $k_{\Delta\text{GH}}$. All experiments in 10 mM lithium cacodylate buffer (pH 7.3) with 100 mM KCl. For titration data for **HL-OH(R)** see Figure S8.

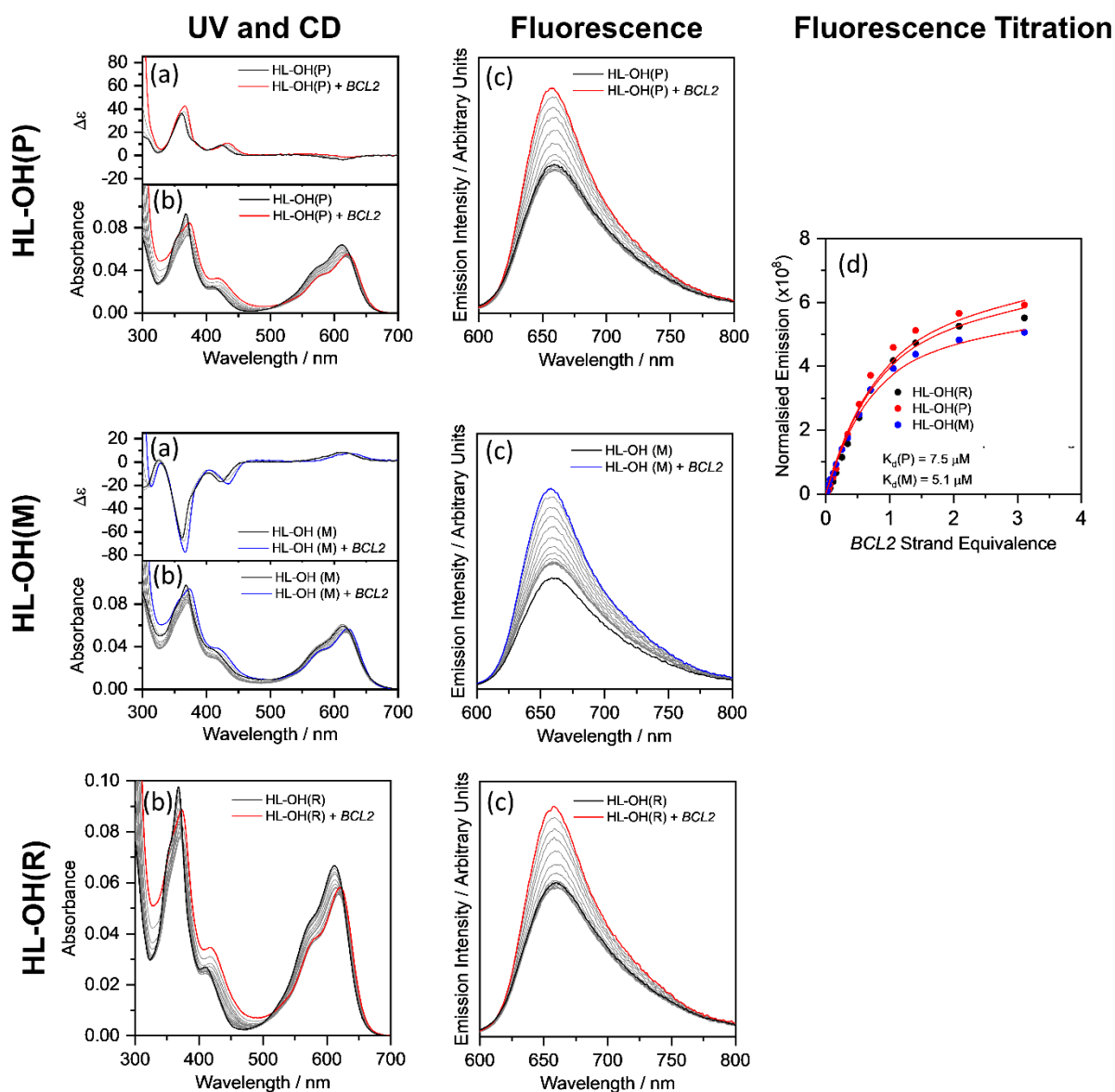


Figure S16. Titration spectra and competitive binding affinities of HL-OH(R) (6 μM , 0% ee), HL-OH(P) (6 μM , 32% ee), and HL-OH(M) (6 μM , 96% ee) to BCL2. (a) CD spectra during addition of BCL2. (b) Absorption spectra and (c) Fluorescence spectra ($\lambda_{\text{exc}} = 580 \text{ nm}$, $\lambda_{\text{em}} = 600\text{-}700 \text{ nm}$) during addition of BCL2. (d) Difference in Integrated emission during titration. Integrated intensities are normalised against absorption at the excitation wavelength. The solid red lines are a simultaneous best fit of all three titrations to a competitive binding model, to solve for K_P , K_M , $k_{\Delta\text{GP}}$ and $k_{\Delta\text{GH}}$. All experiments in 10 mM lithium cacodylate buffer (pH 7.3) with 100 mM KCl.

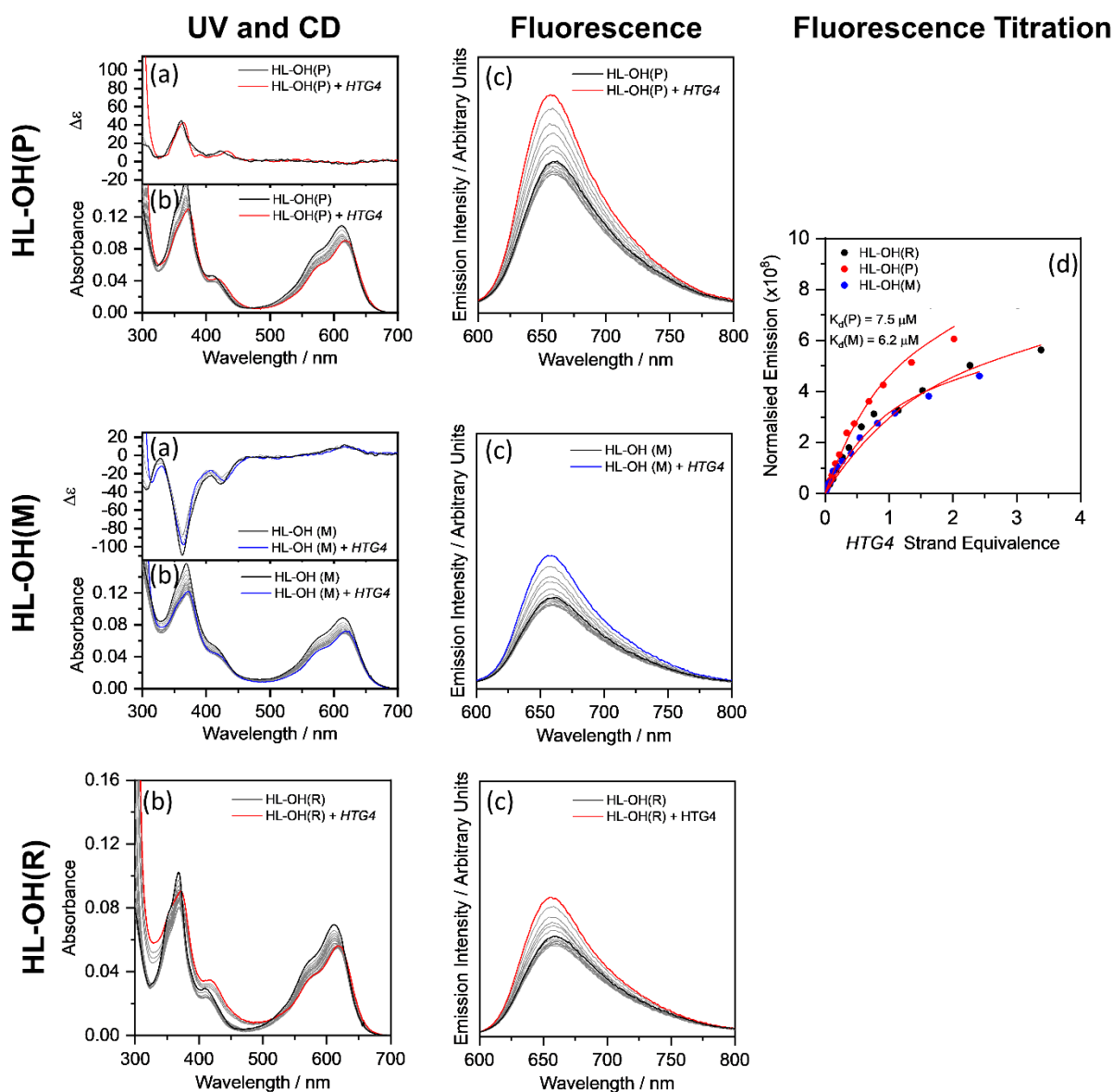


Figure S17. Titration spectra and competitive binding affinities of **HL-OH(R)** (6 μM , 0% ee), **HL-OH(P)** (10 μM , 32% ee), and **HL-OH(M)** (8 μM , 96% ee) to *HTG4*. (a) CD spectra during addition of *HTG4*. (b) Absorption spectra and (c) Fluorescence spectra ($\lambda_{\text{ex}} = 580 \text{ nm}$, $\lambda_{\text{em}} = 600\text{-}700 \text{ nm}$) during addition of *HTG4*. (d) Difference in Integrated emission during titration. Integrated intensities are normalised against absorption at the excitation wavelength. The solid red lines are a simultaneous best fit of all three titrations to a competitive binding model, to solve for K_P , K_M , $K_{\Delta GP}$ and $K_{\Delta GH}$. All experiments in 10 mM lithium cacodylate buffer (pH 7.3) with 100 mM KCl.

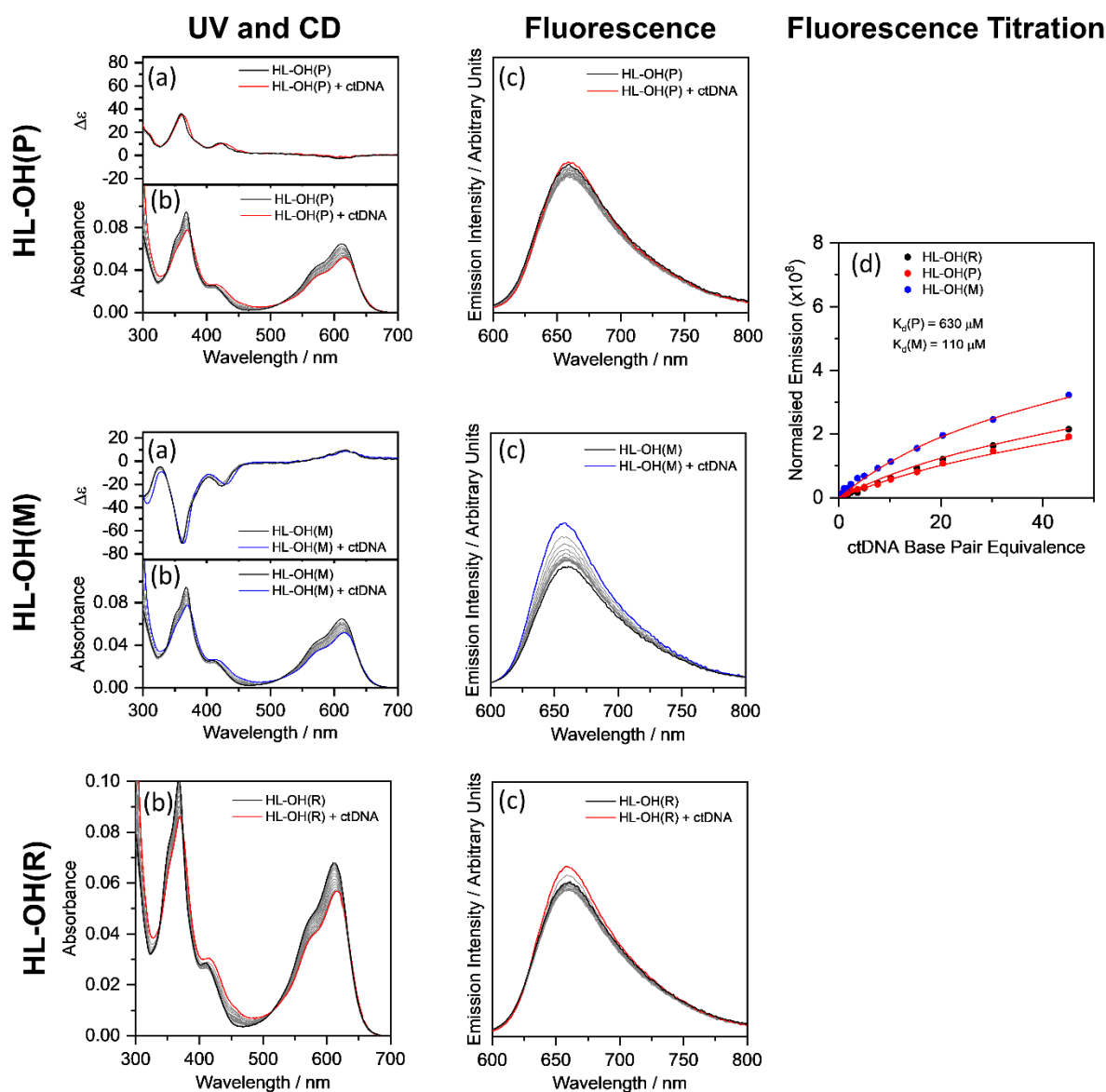


Figure S18. Titration spectra and competitive binding affinities of **HL-OH(R)** (6 μM , 0% ee), **HL-OH(P)** (6 μM , 32% ee), and **HL-OH(M)** (6 μM , 96% ee) to ctDNA. (a) CD spectra during addition of ctDNA. (b) Absorption spectra and (c) Fluorescence spectra ($\lambda_{\text{ex}} = 580 \text{ nm}$, $\lambda_{\text{ex}} = 600\text{-}700 \text{ nm}$) during addition of *c-Myc*. (d) Difference in Integrated emission during titration. Integrated intensities are normalised against absorption at the excitation wavelength. The solid red lines are a simultaneous best fit of all three titrations to a competitive binding model, to solve for K_P , K_M , $k_{\Delta\text{GP}}$ and $k_{\Delta\text{GH}}$. All experiments in 10 mM lithium cacodylate buffer (pH 7.3) with 100 mM KCl. For titration data for **HL-OH(R)** see Figure S9.

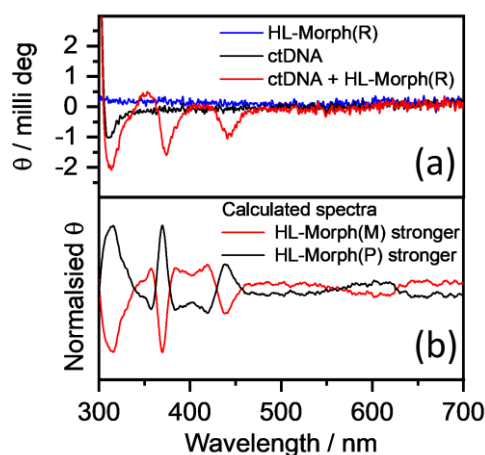


Figure S19. (a) CD Spectra of **HL-Morph(R)** (15 μ M, blue line), ctDNA (1.67 mM, black line) and a mixture of **HL-Morph(R)** and ctDNA (10 μ M and 1.67 mM, respectively, red line). (b) Calculated spectra assuming either **HL-Morph(M)** or **HL-Morph(P)** is more strongly bound to ctDNA. Calculation based on the CD spectra of **HL-OH(M)** when bound to ctDNA and free in solution [see Figure S18(a)].

As can be seen in Figure S18(a), as ctDNA is added to **HL-OH(M)** the magnitude of the negative CD bands remains almost constant and there is a small red shift. We do not assign this small change in the CD signal to a new chiral arrangement, but rather to a slightly different molecular environment and so altered electronic transition. Essentially, this change is reflected in a small shift in the absorption spectra upon binding to ctDNA [Figure S18(b)].

As it was almost enantiomerically pure (96% ee), we were able to measure the CD spectra of unbound, and ctDNA bound **HL-OH(M)** [Figure S18(a)]. The corresponding CD spectra of **HL-OH(P)** can be estimated from the opposite ellipticity of **HL-OH(M)**. Using these spectra we were able to predict the expected change in the CD signal of **HL-OH(R)** if either the M or the P isomers were to bind to ctDNA more strongly. This result is presented in Figure S19(b). It can be seen that the M isomer binding more strongly clearly recreates the observed spectral pattern more closely than if the P isomer was more strongly bound.

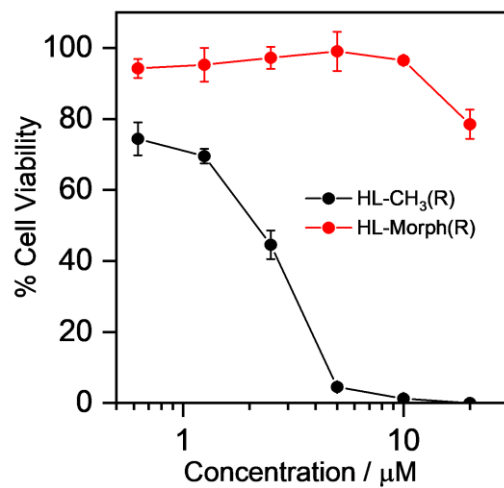


Figure S20. Cytotoxicity of **HL-Morph(R)** and **HL-CH₃(R)** towards U2OS cells at 24 hr. Error bars are the \pm SD of three measurements.

Additional fluorescence lifetime data:

We have measured the fluorescence lifetimes (τ_w) for enantio-enriched and racemic mixtures of **HL-OH** upon binding to *c-Myc* and *BCL2* G4s (Table S1). While slightly higher lifetimes were detected for the **HL-OH(P)** isomer (which we were not able to purify above 32% ee), compared to **HL-OH(R)** (0% ee) and **HL-OH(M)** (96% ee), we note that there is a more significant variation between lifetimes upon binding to different G4s (*BCL2* > *c-Myc*), as well as the pH dependence of the fluorescence lifetime of all the compounds (Table S2). Thus, we did not examine the lifetime differences for enantiopure/enriched compounds using FLIM. However, we have recorded FLIM of **HL-Morph(R)**, to confirm its binding to DNA *in cellulo*, Figure S21.

Table S1. Fluorescence lifetime (τ_w) of **HL-OH(R)**, **HL-OH(M)**, and **HL-OH(P)** in 10 mM lithium cacodylate buffer (pH 7.3) with 100 mM KCl observed upon binding to excess of G4 DNA.

	Lifetime (τ_w) / ns	
	<i>c-Myc</i>	<i>BCL2</i>
HL-OH(R) (0% ee)	8.7	9.4
HL-OH(M) (96% ee)	8.2	9.2
HL-OH(P) (32% ee)	9.1	9.6

Table S2. Fluorescence lifetime (τ_w) of **HL-CH₃(R)**, **HL-Morph(R)**, **HL-OH(R)**, **DAOTA-Morph** and **DAOTA-CH₃** and pH 7.3 and pH 1.0 in 10 mM lithium cacodylate buffer with 100 mM KCl.

	Lifetime (τ_w) / ns	
	pH 1.0	pH 7.3
HL-CH₃(R)	5.1	5.1
HL-Morph(R)	7.1	2.6
HL-OH(R)	2.5	3.8
DAOTA-Morph	18.3 ^a	2.5 ^b
DAOTA-CH₃	17.8 ^c	17.8 ^c

^a Value from reference 5 in 0.1 M HCl. ^b Value from reference 6. ^c Value from reference 7 in 0.1M HCl.

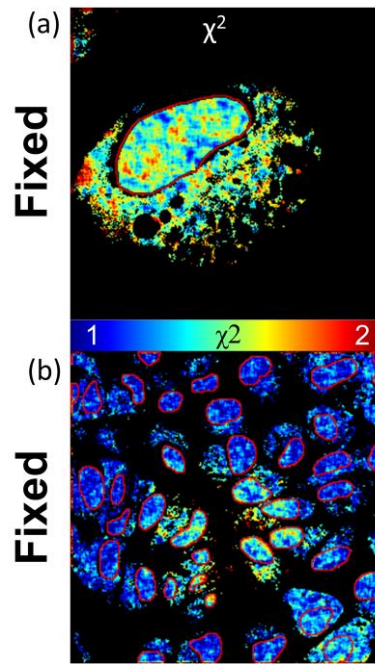


Figure S21 FLIM analysis of fixed U2OS cells stained with **HL-Morph(R)** (20 μ M, 0.5 h, $\lambda_{\text{ex}} = 640$ nm, $\lambda_{\text{em}} = 650\text{-}790$ nm). χ^2 maps of the FLIM images shown in Figure 4, recorded at (a) 512 x 512 and (b) 256 x 256 resolution.

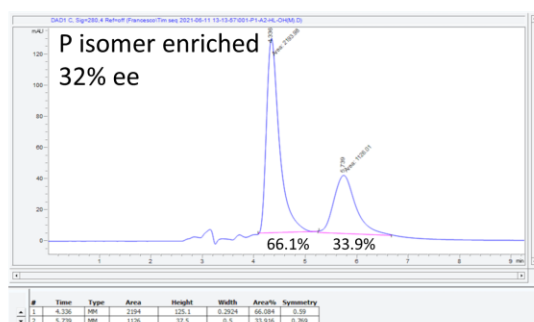
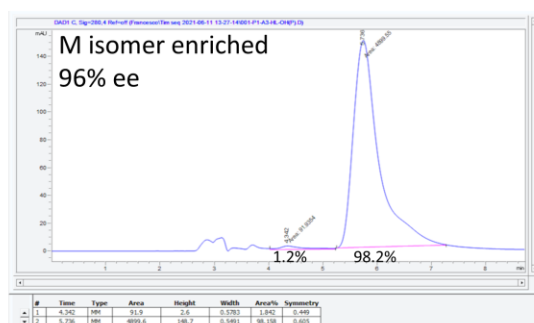
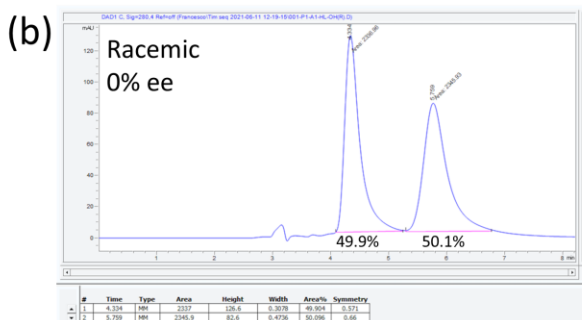
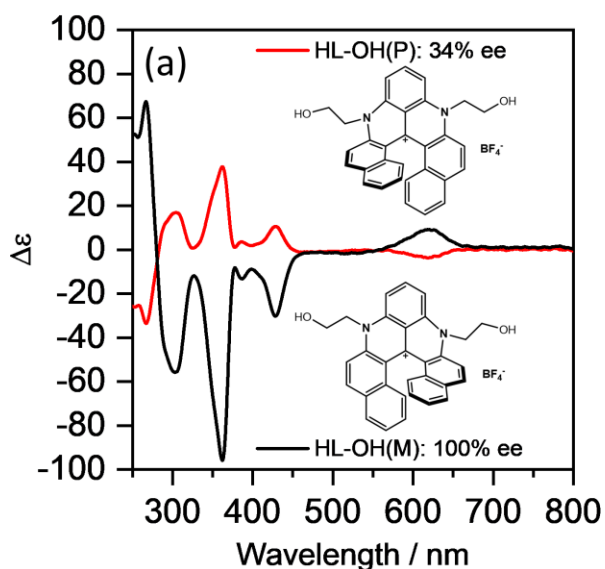


Figure S22. (a) CD Spectra of **HL-OH(P)** and **HL-OH(M)** (12 μM) in CH_2Cl_2 . Calculations of enantiomeric excess (ee) are based on the molar circular dichroism ($\Delta\epsilon$) values for **HL-CH₃(P)** (107 $\Delta\epsilon$, 96 % ee) and **HL-CH₃(M)** ($-87.3 \Delta\epsilon$, 92 % ee) in reference 8. (b) Chiral HPLC trace of **HL-OH(R)**, **HL-OH(P)** and **HL-OH(M)** immediately following reduction using NaBH_4 . Calculations of (ee) are based on the integrated peak areas.

References

1. P. Thordarson, *Chem. Soc. Rev.*, 2011, **40**, 1305-1323.
2. P. Thordarson, *Chem. Soc. Rev.*, 2011, **40**, 5922-5923.
3. I. Jarmoskaite, I. AlSadhan, P. P. Vaidyanathan and D. Herschlag, *eLife*, 2020, **9**, Article e57264.
4. Z. X. Wang, *FEBS Lett.*, 1995, **360**, 111-114.
5. A. Shivalingam, M. A. Izquierdo, A. L. Marois, A. Vyšniauskas, K. Suhling, M. K. Kuimova and R. Vilar, *Nat. Commun.*, 2015, **6**, 8178.
6. P. A. Summers, B. W. Lewis, J. Gonzalez-Garcia, R. M. Porreca, A. H. M. Lim, P. Cadinu, N. Martin-Pintado, D. J. Mann, J. B. Edel, J. B. Vannier, M. K. Kuimova and R. Vilar, *Nat. Commun.*, 2021, **12**, 162.
7. A. Shivalingam, A. Vysniauskas, T. Albrecht, A. J. P. White, M. K. Kuimova and R. Vilar, *Chem. – Eur. J.*, 2016, **22**, 4129-4139.
8. F. Torricelli, J. Bosson, C. Besnard, M. Chekini, T. Burgi and J. Lacour, *Angew. Chem., Int. Ed.*, 2013, **52**, 1796-1800.